# Neutron-Production Double-Differential Cross Sections for 150 MeV Neutron-Incidence on Fe

Hiroyuki Arakawa[1], Tsuyoshi Kajimoto[1], Shusaku Noda[1], Takehito Watanabe[1], Nobuhiro Shigyo[1], Kenji Ishibashi[1], Satoshi Kunieda[2], Robert C. Haight[3],

[1] Kyushu University, 744, Motooka, Nishi-ku, Fukuoka 819-0395 Japan

[2] Japan Atomic Energy Agency, Tokai, Naka, Ibaraki 319-1195 Japan

[3] Los Alamos National Laboratory, Los Alamos, NM 87545 USA

The neutron-production double-differential cross sections for the neutron-induced reaction were measured on Fe at 140 – 160 MeV. Neutrons produced by a 800 MeV proton-bombarded spallation target were used as incident particles. The results are compared with calclated data.

## 1 Introduction

High-energy neutron production double-differential cross sections are important for realization of accelerator driven systems (ADS) and radiotherapy. Proton-induced neutron-production double-differential cross sections have been measured up to 3 GeV. However, data of neutron-induced neutron-production double-differential cross sections above 100 MeV are insufficient because of neutron measurement difficulties and a few quasi-monochromatic neutron sources. Utilization of a continuous energy neutron source by spallation reaction enables us to measure cross section for various incident energies at a time.

The purpose of this study is to measure the neutron-production double-differential cross sections at 150 MeV on Fe using a continuous energy neutron source.

## 2 Experiments

Experiments were performed at the Weapons Neutron Research (WNR) facility in Los Alamos Neutron Science Center (LANSCE)[1)] which has an 800 MeV proton linear accelerator. Neutrons generated at a tungsten spallation target (Target-4) were used as incident particles. The neutron energies cover a wide energy range up to 750 MeV. The distance between the spallation target and the experimental room is about 90 m. The geometry of the WNR facility is illusrated in Fig. 1.

Experiments consist of 2 parts. One part was the measurement of response functions of neutron detectors. The energy spectra of emitted neutrons were derived from unfolding their deposition-energy spectra with the responses of the detectors. These response functions were measured by using the spallation neutrons which were collimated to 2 mm in diameter. The alignent of the experiment is in Fig. 2. The response function of each NE213 liquid organic scintillator 12.7 cm thick and 12.7 cm in diameter was measured by irradiating neutrons from the Target-4. The time-of-flight (TOF) between the spallation target and a neutron detector and the charge spectrum from the photomultiplier connected with the NE213 scintillator were measured.

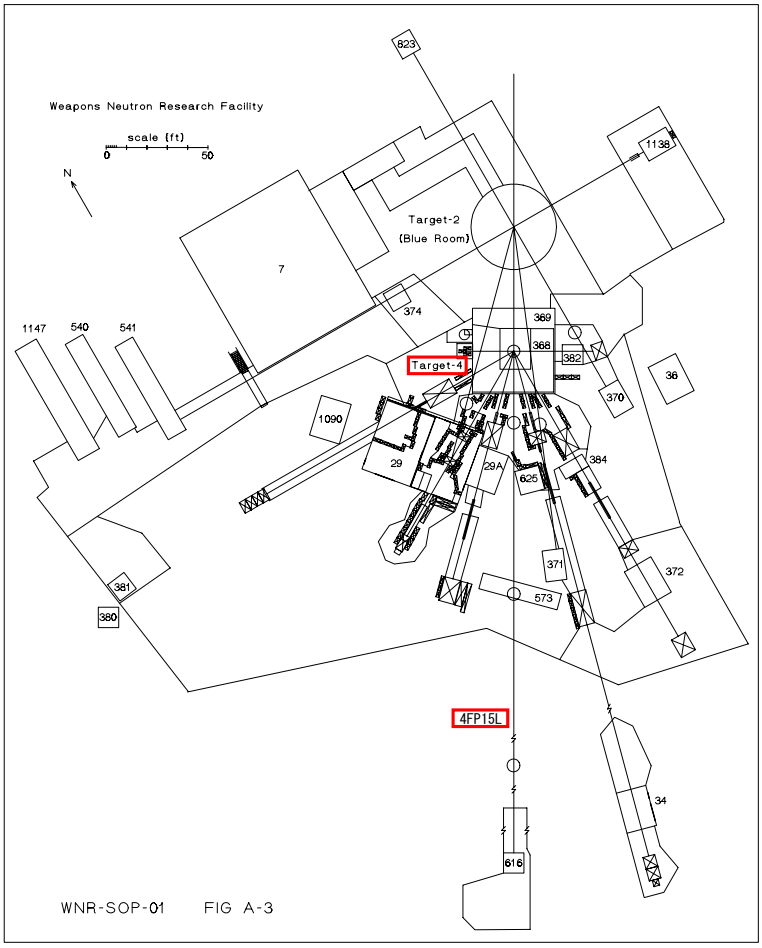


Fig. 1. Schematic view of the beam line at the WNR facility[2)]

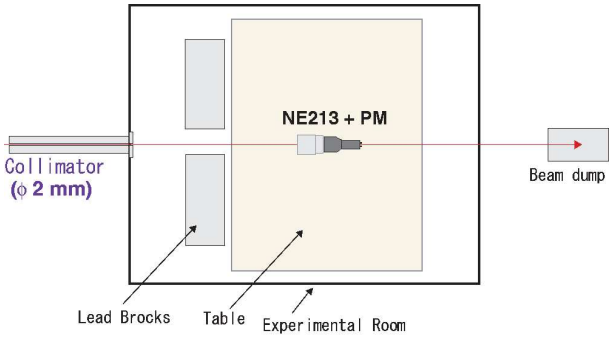


Fig. 2. Arrangement of the measurement for response function

Another part of the experiment was the measuremnt of double-differential cross sections. Setup of the measurement are shown in Fig. 3.

Six NE213 scintillators were employed to detect neutrons emitted from an Fe sample (10 mm thick, $\phi$50 mm) and placed at 15°, 30°, 60°, 90°, 120° and 150°. The distance between the sample and the detectors were about 0.7 m. A fission ionization chamber[3)] was set to know the incident-neutron flux. A 10 mm thick NE102A plastic

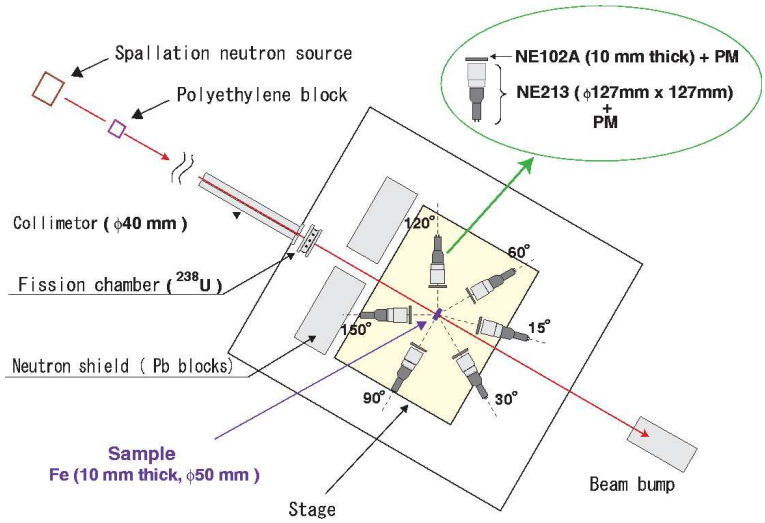


Fig. 3. Set up of the measurement for deposition-energy spectra

scintillator as a veto detector was set in front of each NE213 scintillator. The beam size was adjusted to 36 mm in diameter.

## 3 Analysis

### 3.1 Elimination of charged particles and gamma rays

Charged particle events were eliminated by discrimination of signals from an NE102A scintillator plastic scintillators because charged particles gave larger energy in an NE213 scintillator than neutrons and gamma-rays. An example of ADC spectra by an NE102A plastic scintillator is shown in Fig. 4.

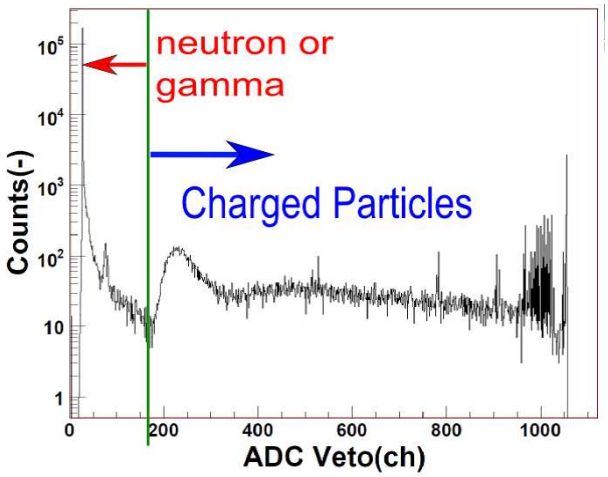


Fig. 4. An example of ADC spectrum of a veto detector

Gamma-ray events were discriminated using the two gate integration method[4] since NE213 liquid organic scintillators were sensitive to not only neutrons but also gamma rays. Fig. 5 stands for schematic view of the gate

integration method. Comparison between ADC spectrum with the prompt-gate and that with the delayed-gate enables to discriminate between neutron events and gamma ray ones. Fig. 6 illustrates an example of the 2D-plot of the ADC spectra with the prompt gate and the delayed one.

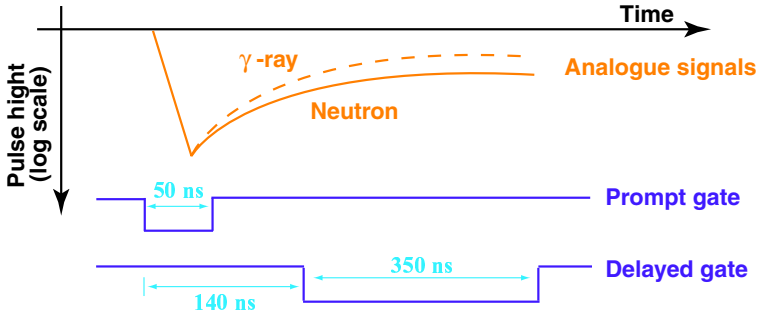


Fig. 5. Schematic view of gate integration method

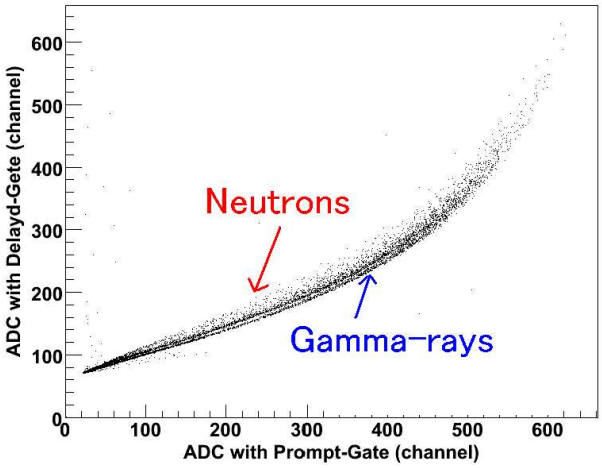


Fig. 6. Discrimination of neutrons and gamma rays

### 3.2 Incident neutron energy

Incident neutron energies were obtained by neutron flight times between Target-4 and NE213 scintillators. Because the distance between Target-4 and the sample were much longer than those between the sample and the detectors, the flight time of the latter was negligible. Fig. 7 shows a schematic view of the TOF measurement alignment. The timing of flash gamma-rays from the spallation target was used as the time base of TOF analysis. Fig . 8 shows one of TOF spectra.

### 3.3 Incident neutron flux

The number of incident neutrons was possible to be gotten by the equation

$$\phi_{\mu p}(E_n)\Delta E_n = \frac{n_f(E_n)\Delta E_n}{\sigma(E_n) \times \epsilon_{eff} \times \rho_f} \times \frac{1}{n_{\mu p} \times S_{beam}} \quad (1)$$

where $\phi_{\mu p}(E_n)$, $n_f(E_n)$, and $\sigma(E_n)$ are the number of incident neutron flux, the number of fission events detected by the fission chamber, and the fission cross sections of $^{238}$U for corresponding neutron energy $E_n$ [5], respectively.

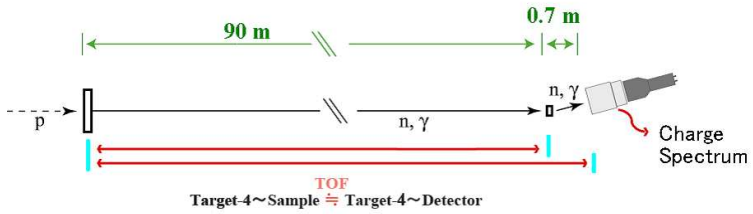


Fig. 7. Schematic view of the TOF measurement alignment

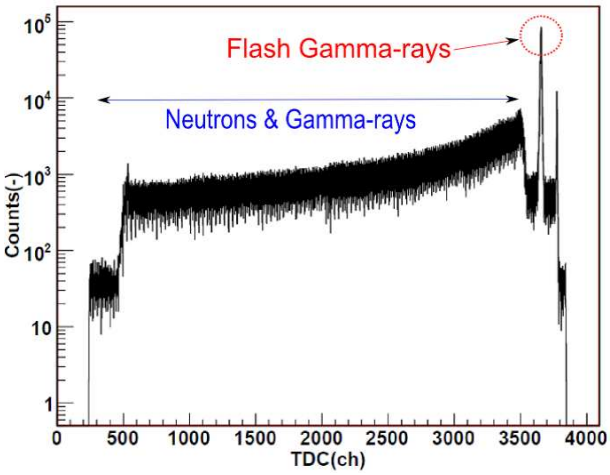


Fig. 8. TOF spectrum between the spallation target and a neutron detector

$\epsilon_{eff}$is the detection efficiency of the fission chamber, and $\rho_f$ is the arial density of the number of atoms of fissile material on the foil in chamber. $S_{beam}$ is the cross section of the beam.

### 3.4 Calibration

Charge-integration spectra were calibrated to get corresponding electron-equivalent light-output for all neutron detectos. The gamma-ray Compton edges of $^{60}$Co and Pu-Be sealed sources were converted into light-unit with the semi-empirical formula by Dietze et al.[6] for low-energy (a few MeV) parts. For the calibrations of higher-energy, neutron energies were identified by the TOF between the spallation target and neutron detectors and were converted into light-unit by the empirical equation by Cecil et al.[7]

$$T_e = 0.83T_p - 2.82[1.0 - exp(-0.25T_p0.93)] \tag{2}$$

where $T_p$, $T_e$ are proton and electron energy in an NE213 scintillator, respectively. The maximum channel of the ADC spectrum was used as corresponding charge-integration values. The relationship between charge-integrations and electron-equivalent light-outputs for the NE213 scintillator used at 90° is shown in Fig. 9

### 3.5 Response functions and Deposition-energy spectra

Response functions normalized by the number of incident-neutrons were shown in Fig. 10. In this experiment, the SCINFUL-QMD[8] calculations adjusted to reproduce experimental data with light attenuation were used as

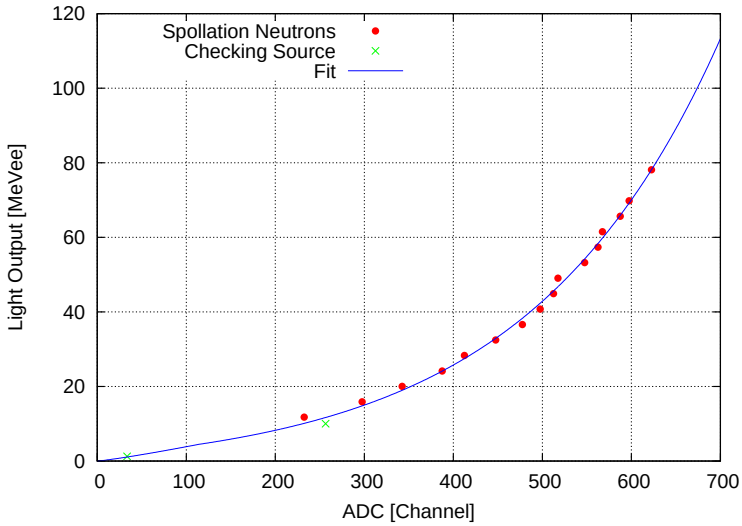


Fig. 9. Relationship between integrated charge and light output for 60° detector

response matrix elements below 30 MeV incident energy for all neutron detectors since there are no experimental data below 30 MeV incident energies.

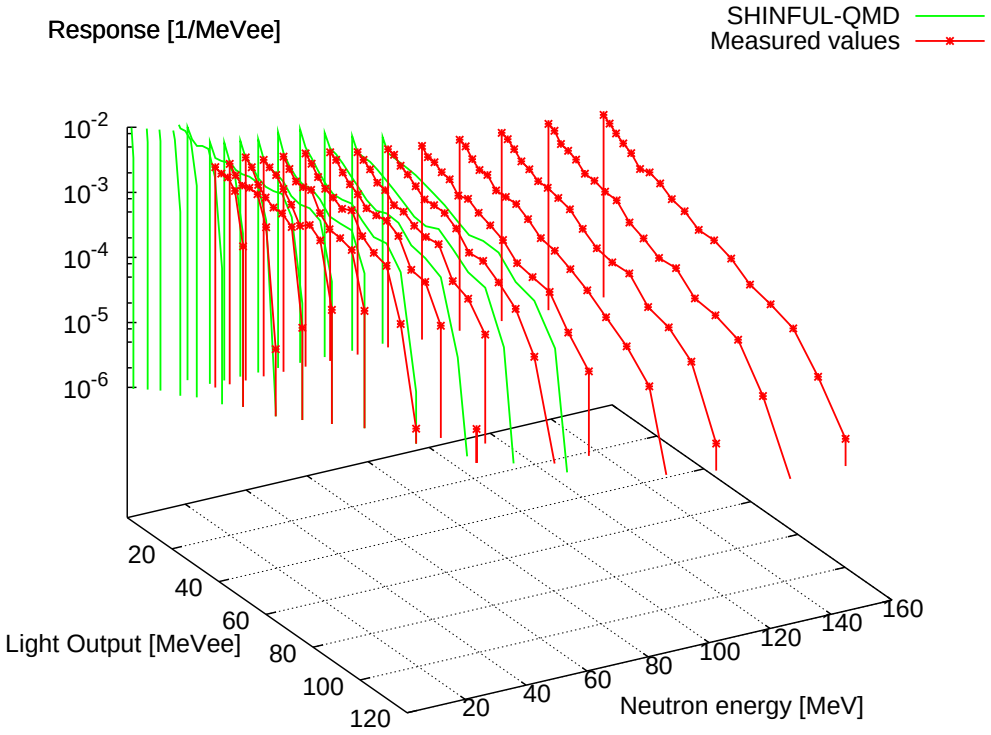


Fig. 10. Response functions of the NE213 scintillator at 60°

Deposition-energy spectra at 140 – 160 MeV normalized by the number of incident-neutrons and subtracted

background (sample-out) spectra are shown in Fig. 11.

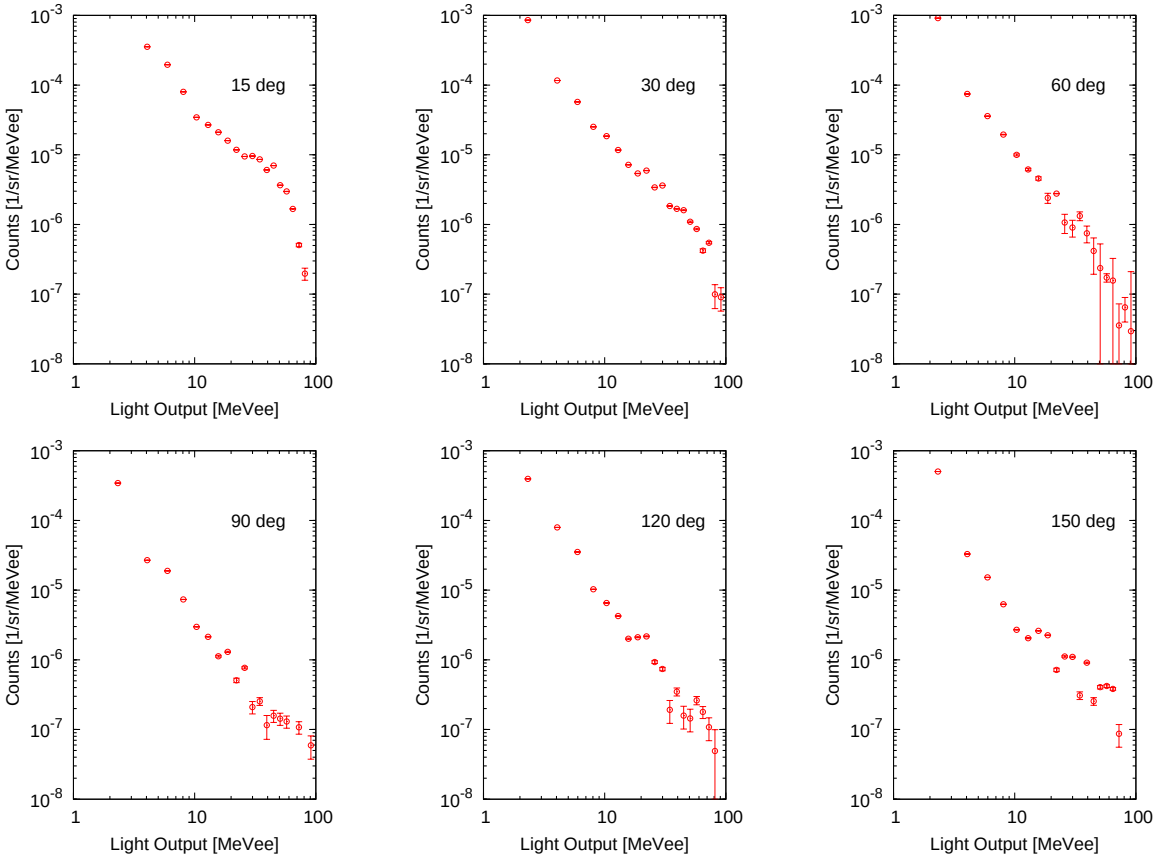


Fig. 11. Deposition energy spectra at 140 – 160 MeV neutron incident energy

### 3.6 Unfolding

The energy spectra of emitted neutrons were derived by unfolding their deposition-energy spectra with the responses of the detectors. In this experiment, elastic scattering component was considered separatly from the other reaction ones. The determinant of this experiment was

$$\begin{pmatrix} \vdots \\ y_\xi \\ \vdots \end{pmatrix} = \begin{pmatrix} \ddots & \vdots & \vdots \\ \vdots & a_{\xi,E} & \vdots \\ \vdots & \vdots & \ddots \end{pmatrix} \cdot \begin{pmatrix} \vdots \\ x_E \\ \vdots \end{pmatrix} \cdot k + \begin{pmatrix} \vdots \\ a_{\xi,E_{in}} \\ \vdots \end{pmatrix} \cdot x_{el} \cdot k \tag{3}$$

where $y_\xi$, $a_\xi$, $E$, and $x_E$ were deposition-energy spectra, response function, outgoing energy spectra (unfolding results), respectively. $x_{el}$ was elastic scattering factor. $k$ was matting factor for absolute value of response functions with deposition-energy spectra. $x_E(=x(E,\theta))$ was assumed to conform following equation.

$$\left(\frac{d^2\sigma}{dEd\Omega} =\right) \frac{x(E,\theta)}{\rho\Delta E} = \sum_{i=1}^{3} pA_i \exp\left\{-\left(\frac{E+m-p\beta_i\cos\theta}{\sqrt{1-\beta_i^2}} - m\right)\right\} \tag{4}$$

where $E$ and $p$ is the kinetic energy (MeV) and the momentum (MeV/c) of an emitted neutron in the laboratory frame and $m$ the neutron mass (MeV), respectively. The quantities of $A$, $\beta$, and $T$ are called amplitude, velocity

and temperature parameters, respectively. Three components of $i$ =1 to 3 correspond to individual processes of the cascade, the preequilibrium and the evaporation. In the process of unfolding these deposition-energy spectra, neutron-induced neutron-production double-differential cross sections were parameterized with moving source model by SALS code[9] as a least mean square approximation program.

## 4 Results

The provisional parameterized double-differential cross sections by the moving source model with it's elements as experimental results for 140 – 160 MeV neutron incident energy are shown in Fig. 12. These results were compared with the PHITS[10] calculation data, the evaluated value of LA150[11](GNASH[12]+ Kalbach and Mann's systematics[13] ) and JENDL-HE[14]. The experimental results show that under 50 MeV neutron emission energy are approximately good agreement with calculated data except for 15° and 30° results. 15° and 30° experimental results overestimate calclation data from 5 MeV to 100 MeV neutron emission energy and underestimated above that. For backward angles of experimental results over 50 MeV neutron emission energy have some discrepancies with calclation data.

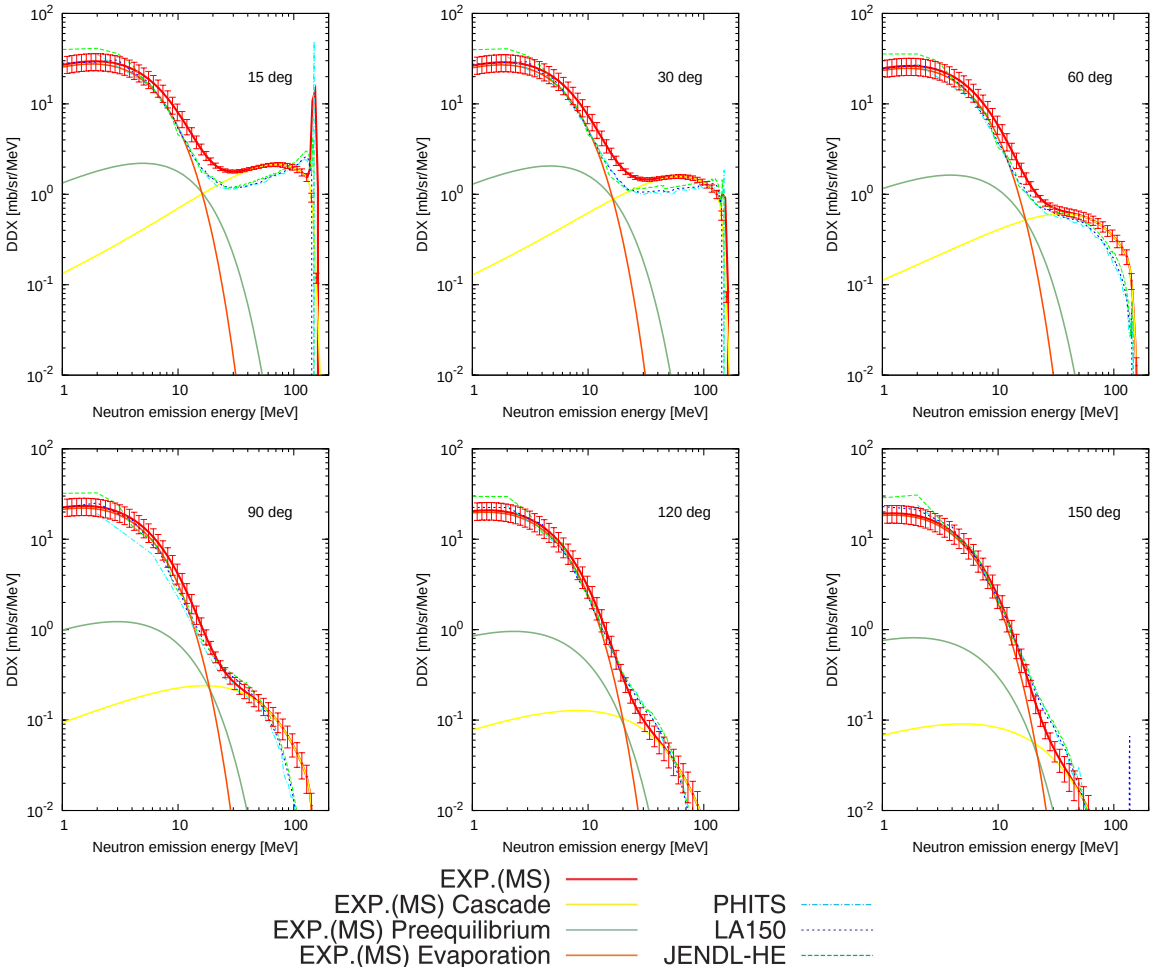


Fig. 12. Double-Differential Cross Sections for 140 – 160 MeV neutron incident energy with calclated data

## 5 Conclusion

The neutron-production double-differential cross sections at 150 MeV on Fe are measured using a continuous energy neutron source. The double-differential cross sections were parametalized by moving source model. The experimental results have some discrepancies with calculated data. To understanding these discrepancies, for more detailed analysis are needed.

References


1) P.W. Lisowski, C.D. Bowman, G.J. Russell, and S.A. Wender. *J. Nucl. Sci. Eng.*, 106:208, 1990.
2) Weapons neutron research facility (WNR). `http://wnr.lanl.gov/`.
3) S.A. Wender, S. Balestrini, A. Brown, R.C. Haight, C.M. Laymon, T.M. Lee, P.W. Lisowski, W. MacCokle, R.O. Nelson, W. Parker, and N.W. Hill. *J. Nucl. Instrum. Methods Phys. Res.*, A336:226, 1993.
4) M. Moszynsky and et al. *J. Nucl. Instrum. Methods.*, A343:563, 1994.
5) P.W. Lisowski, A. Gavron, W.E. Parker, J.L. Ullmann, S.J. Balestrini, A.D. Carlson, O.A. Wasson, and N.W. Hill. Fission cross sections in the intermediate energy region. *Specialists meeting on neutron cross section standards for the energy region above 20 MeV*, 21:23, 1991.
6) G. Dietze and H. Klein. *J. Nucl. Instrum. Methods.*, 193:549, 1982.
7) R.A. Cecil, B.D. Anderson, and R. Madey. *Nucl. Instr. Meth.*, 161:439, 1979.
8) D. Satoh, N. Shigyo, Y. Iwamoto, H. Kitsuki, and K. Ishibashi. *IEEE Trans. Nucl.Sci.*, 48:1165 – 1167, 2001.
9) T. Nakagawa and Y. Oyanagi. *Recent Developments in Statistical Inference and Data Analysis "Program system SALS for nonlinear least-squares fitting in experimental science" (K. Matsusita, ed.)*, page 221. NorthHolland. Publ. Amsterdam, 1980.
10) H. Iwase and et al. *J. Nucl. Sci. Technol.*, 39:1142, 2002.
11) M.B. Chadwick, P.G. Young, S. Chiba, S.C. Frankle, G.M. Hale, H.G. Hughes, A.J. Koning, R.C. Little, R.E. MacFarlane, R.E. Prael, and L.S. Walter. *Nucl. Sci. Eng.*, 131:293 – 328, 1999.
12) P.G. Young, E.D. Arthur, and M.B. Chadwick. *LA-6947 (1997) ; LAUR-88-382 (1988).*
13) C. Kalbach and F.M. Mann. *Phys. Rev.*, C23:112, 1981.
14) Y. Watanabe, T. Fukahori, K. Kosako, N. Shigyo, T. Murata, N.Yamano, T. Hino, K. Maki, H. Nakashima, N.Odano, and S.Chiba. Nuclear data evaluation for jendl high - energy file. *Proceedings of International Conference on Nuclear Data for Science and Technology ,Santa Fe, New Mexico, USA*, 1:326, Sep.26 - Oct.1 2004.